Ion-irradiation studies of the damage function of copper and silver

R. S. Averback, R. Benedek, and K. L. Merkle

Materials Science Division, Argonne National Laboratory, Argonne, Illinois 60439
(Received 27 December 1977)

A systematic study of the damage function of both Ag and Cu has been performed by measuring resistivity increments induced by irradiation of thin-foil specimens at 6 K with several species of ions. Beam energies were selected such that the projectiles were stopped within the target. Results were compared with theoretical calculations based on a modified Kinchin-Pease damage function. The damage efficiency (ratio of experimental-to-theoretical values) is roughly unity for irradiations with H, but decreases rapidly as the projectile mass increases, which results in harder recoil spectra. For projectiles heavier than Ne, the efficiency becomes relatively constant (0.4 for Ag and 0.35 for Cu). These results indicate that deviations from the modified Kinchin-Pease model begin to occur at energies not far above the displacement threshold energy and the efficiency becomes roughly constant for recoil energies greater than a few keV. Comparison is made with damage-rate studies for other types of irradiation.

I. INTRODUCTION

The determination of the damage (or displacement) function has been a long-standing concern in the field of radiation effects. This function specifies the number of Frenkel pairs produced in a cascade initiated by a lattice-atom recoil of a given energy. The damage produced by energetic neutrons in the structural components of fission and proposed fusion reactors is of considerable practical concern. However, studies of damage production by neutron irradiation have been encumbered by several difficulties. Until recently accurate determinations of neutron spectra and fluence have not been available.[1] Furthermore, extensive calculations,[2] based on the neutron spectrum and the nuclear cross sections, of the primary recoil spectrum and the damage energy are required before experimental data can be compared with theory. Considerable recent progress in both areas[1,2] now enable much more quantitative neutron-damage studies than were possible in the past. One remaining limitation of neutron studies is that the neutron energy spectrum for a given source is relatively fixed. In principle, it would be desirable to compare the damage associated with several spectra to gain a more systematic understanding of the damage function. These considerations have stimulated the investigation of damage production by other types of irradiation.

Electron irradiation in the MeV energy range provides an alternative method of producing radiation damage. Compared with neutron irradiation, it has certain advantages. Intense, monoenergetic, collimated beams of electrons are produced in Van de Graaff accelerators or high-voltage electron microscopes. Dosimetry is more routine and the relevant cross sections are better known

than in the case of neutron irradiation. However, electron irradiation is not useful for the production of highly energetic displacement cascades, since the maximum recoil energy is normally of the order of 100 eV.

Ion beams can also be used to produce radiation damage. As in the case of electron irradiation, the dosimetry is rather routine and projectile-target cross sections are relatively well known. Many ion accelerators have the flexibility to produce beams of virtually any ion species. Previous damage-rate measurements for ion irradiation[3-11] have, for the most part, employed light projectiles, i.e., protons and α particles. By changing the particle energy it is possible to study the effect of the recoil spectrum on defect production.[11] However, the nature of the primary recoil spectrum is more sensitive to the mass than to the energy of the irradiating ion. This aspect of ion irradiation has been utilized in the present work, the aim of which was to obtain a systematic understanding of the damage function. Specifically, we have measured damage rates in Cu and Ag for projectiles that range in mass from 1(H) to 209 (Bi). The proton irradiations, which were performed at ~20 keV, produce low-energy recoils similar to those that occur in electron irradiation. The Bi irradiations (at 720 keV), on the other hand, produce defects mainly in dense high-energy cascades. The ions intermediate in mass give rise to damage states that lie between these extremes.

Two types of ion-beam damage-rate experiments can be distinguished. In one, high-energy beams are transmitted through the specimen foil with relatively small energy loss. This method is normally restricted to light ions. In the other type of experiment (described in the present paper), the projectile energy is such that the beam is stopped

within the specimen. A wide range of projectile masses can be employed under these circumstances. An important distinction exists between the analyses of the two types of ion-beam experiments; in the second type, the stopping power of the projectile has a strong bearing on damage production. Indeed, this feature may be exploited to extract information on the stopping power as well as the damage function.

The damage rates are determined in the present experiments by residual-resistivity measurements on thin-film specimens following irradiation at ~6 K. The measurements were corrected for the electrical-resistivity size effect to permit comparison with bulk values. To test the validity of the correction procedure employed, experiments were performed on foils of several thicknesses. The results were found to be independent of thickness, within experimental error.

The experimental results are analyzed to obtain the number of Frenkel pairs produced per incident ion. This value is compared with a theoretical prediction based on a modified Kinchin-Pease model. Rather similar trends in the efficiency (ratio of experimental-to-theoretical values) are observed for both Cu and Ag. The efficiencies decrease from a value close to unity for proton irradiation to ~0.4 for heavy-ion irradiation. It is suggested that a thermal-spike effect is the most likely explanation of the low efficiencies observed for the high-energy cascades produced by heavy ions.

The experimental procedure is outlined in Sec. II. The theoretical calculations of damage production are described in Sec. III. Results for the damage efficiencies are presented in Sec. IV. In Sec. V, implications of the present results are discussed.

II. EXPERIMENTAL

In the present experiment, thin-foil copper and silver specimens were irradiated successively with ions of different atomic species. For each ion, the energy was selected such that the projected range $\langle R_p \rangle$ was approximately half the specimen thickness. The irradiations and the resistance measurements were carried out at ~6 K; at this temperature the defects are immobile.

The number of Frenkel pairs produced per incident ion is related to measured electrical-resistivity increments by the equation

$$D' \equiv \frac{d\Delta\rho}{d\phi} = \frac{\nu^e}{nt}\rho_F.$$ (1)

Here, $\Delta\rho$ is the radiation-induced change in the electrical resistivity, ϕ is the ion dose, ν^e is the number of defects produced per incident ion, n is the atomic density, t is the specimen thickness, and ρ_F is the resistivity of Frenkel pairs per unit concentration.

Both single and polycrystalline specimens were produced by vapor deposition onto rocksalt in an ultrahigh-vacuum chamber with a pressure of ~10^{-10} Torr before evaporation and ~10^{-7} Torr during evaporation. The specimens were grown from 99.9999% pure starting materials. Specimen thicknesses were determined by a crystal monitor during growth and afterwards by gravimetry. Only those specimens for which both techniques yielded similar results were retained. The more accurate gravimetry determinations of thickness were employed in Eq. (1). The principal measurements were made on specimens with a thickness of $(2-3)\times 10^{-5}$ cm, although tests were made on somewhat thicker specimens, as described in Sec. IV.

Using a masking technique, the specimens were grown with the potential and current leads attached. The mask design provides for four gauge lengths in each specimen, each of which could be separately irradiated. The lateral dimensions of the specimen are approximately 0.025×0.10 cm. The geometry factor that relates resistance to resistivity can be calculated from the measured resistance of the specimen at $0°C$. Residual resistivity ratios for the specimens were typically in the range 10-30.

The electrical resistance was measured by standard four-probe direct current (dc) potentiometric techniques using a Vidar 521 integrating digital voltmeter (DVM) and Dana preamplifiers. The voltage sensitivity of this system was $\leqslant 1 \times 10^{-7}$ V, which, for the present experiments, corresponds to a resistivity of ~2×10^{-11} Ω-cm or ~0.1-ppm defect concentration. The ion dose was determined by integrating the ion current collected on an annular disk that intercepted a portion of the beam. Appropriate biasing plates were used to suppress the escape of secondary electrons from the ion collector. The ion beam was collimated with 1.0-mm-diam apertures and then rastered over a 1.0-cm² area. This procedure ensured a homogeneous beam intensity over the entire area (0.1 cm²) of the specimen and the Faraday cage. A comparison of the flux measured with a Faraday cup behind the Faraday cage with that measured on the cage showed agreement to ~1% when the beam was rastered. This test was carried out for a wide range of projectile energies and also for multiply charged ions. The current integrator and Vidar DVM were interfaced to a computer so that the damage rates could be determined immediately following each irradiation.

The irradiation chamber was pumped with sorption-roughing pumps and an ion pump. The pressure during irradiation was $\sim 10^{-8}$ Torr. Two radiation shields surrounding the specimens (an outer shield at 78 K and an inner shield at ~ 6 K) minimized both the heat input and the condensation of residual gas on the foils. The orientation of the foil normal, relative to the ion-beam direction, was $\sim 10°$ in altitude and $\sim 5°$ in azimuth. Rotation of the specimen normal from the beam axis is necessary to eliminate the possibility of channeling, even for the polycrystalline specimens, since preferred orientations of the microcrystals relative to the film normal may exist. The specimens, which were grown on rocksalt, were transferred to anodized aluminum substrates for irradiation. The anodization layer provided insulation between the specimen and substrate; however, it was sufficiently thin so that its breakdown voltage was low, $\lesssim 200$ V in air. Since the lowest ion-beam energy used was 30 keV, charging of the substrate during irradiation was insignificant. Tests were performed to verify that no beam heating occurred during the irradiations. The maximum power input by joule heating that caused no detectable temperature rise (as determined by changes in the electrical resistivity of the specimens) was determined. The power input due to the ion beam was kept well below that maximum power.

To convert measured thin-film resistivities to values appropriate to bulk metals, a correction for the size effect is required.[12] In the present work, the size effect was treated as follows. It is noted that the damage rate $d\Delta\rho/d\phi$ for electron irradiation[13] of bulk copper specimens is linear in $\Delta\rho$ to large values of $\Delta\rho$. Proton irradiation produces damage similar to that obtained by electron irradiation. It was therefore assumed that the damage rate for test irradiations with 150-keV protons, corrected for size effect, is linear in $\Delta\rho$. (Although electron-irradiation damage-rate studies are not available for silver, neutron damage-rate curves are essentially linear for this metal.[14]) The Fuchs-Sondheimer theory[15] was employed to correct measured damage rates for 150-keV proton irradiations. Two parameters in the theory, the specularity and the electron density, were adjusted to obtain a linear dependence of the corrected damage rate. This correction established an absolute damage rate for 150-keV protons. Several specimens with different thicknesses and resistance ratios, both single and polycrystalline, were irradiated with 150-keV protons, and the damage rates were corrected in the above manner. The size-effect correction at $\Delta\rho = 0$ for these specimens ranged from $\sim 20\%$ to $\sim 250\%$; however, the corrected damage rates at $\Delta\rho = 0$ were reproduci-

ble to $\pm 10\%$. As described below, all damage rates are normalized to a "standard" corrected damage rate for 150-keV protons. A value for the latter quantity was determined by averaging the results obtained for several specimens with a thickness of $\sim (2-3) \times 10^{-5}$ cm. (For thicker specimens, higher-energy proton irradiations were employed for normalization purposes.)

The size-effect correction for the projectiles of interest in the present study was made by applying the same correction as that obtained for the 150-keV proton irradiation. In practice, this was accomplished by measuring the damage rate for 150-keV protons, measuring the damage rate for two other projectiles, and then remeasuring for the 150-keV protons. If D_S^P is the "standard" damage rate (obtained as described above), D_N^P is the measured damage rate for 150-keV protons, and D is the damage rate measured for the projectile of interest, the corrected damage rate is then given by

$$D' = D_S^P D / D_N^P .$$

This procedure was repeated until roughly ten damage rates were measured for each specimen. To minimize uncertainties associated with radiation-annealing effects, only a limited number of irradiations were performed on a given specimen. Equation (1) applies only at $\Delta\rho = 0$, i.e., before any damage has been introduced into the specimen. At finite but not too large $\Delta\rho$, the damage rate can be expressed as

$$\frac{d\Delta\rho}{d\phi} = \rho_F \frac{v^e}{nt} \left(1 - \frac{2\Omega_r \Delta\rho}{\Omega_0 \rho_F}\right), \tag{2}$$

where Ω_r is the effective spontaneous recombination volume[16] and Ω_0 is the atomic volume. If Ω_r were the same for all types of irradiation, the normalization procedure outlined above would correct for size effects as well as for radiation annealing. However, since Ω_r depends somewhat on the type of irradiation,[17,18] the following procedure was adopted to account for radiation-annealing effects. A 150-keV proton damage rate was obtained to determine the size-effect correction. Next, a damage rate for 300-keV Ar was measured and corrected for the size effect, using the 150-keV proton damage rate. The Ar irradiations were then alternated with heavy-ion ($M_i \geqslant 12$) irradiations; correction for radiation annealing was made by normalizing the heavy-ion damage rates to those obtained for Ar. Thus we write $D' = D_S^P D_N^{Ar}(0)$ $D(\Delta\rho)/D_N^P(0) D_N^{Ar}(\Delta\rho)$, where $D_N^{Ar}(0)$ is the measured Ar damage rate in the undamaged specimen and $D_N^{Ar}(\Delta\rho)$ is that obtained when the radiation-induced resistivity is $\Delta\rho$. After the heavy-ion irradiations were completed, the light-ion irradiations were performed, using 150-keV proton irradiations for

normalization. The resistivity increment for each irradiation step was $\Delta\rho \sim 1.5 \times 10^{-9}$ Ω-cm. The normalization procedures described above were found reliable when $\Delta\rho \lesssim 5 \times 10^{-8}$ Ω-cm or ~10% of the saturation defect concentration.[17] Thus, damage rates obtained after correcting for both size effect and radiation annealing were observed to be independent of $\Delta\rho$ when the total damage-induced resistivity was within this range.

Finally, two assumptions inherent in Eq. (1) deserve discussion. Values of the resistivity per unit concentration of Frenkel pairs ρ_F were taken from a compilation by Lucasson based on electron-irradiation studies.[19] In the analysis of the present experiment, it is assumed that ρ_F is the same for all types of irradiation. The available evidence indicates that the errors incurred by the above assumption are small. Without giving an exhaustive discussion, we mention two experiments that support this assumption. First, simultaneous measurements of resistivity change $\Delta\rho$ and lattice parameter change Δa have been carried out during low-temperature neutron irradiation[20] and electron irradiation[21] of Cu. The ratio $\Delta\rho/(\Delta a/a)$ was identical, to within ~5%, for the two types of irradiation. Furthermore, the ratio remained unchanged during annealing. In the other experiment,[22] diffuse x-ray scattering and electrical resistivity were measured simultaneously during isochronal annealing after electron irradiation. Analysis of the diffuse x-ray scattering indicated that, during stage II in Cu and Al, the interstitials agglomerate to form clusters. On the other hand, the residual resistivity was nearly constant over a substantial portion of the annealing stage. The above-mentioned experiments tend to indicate that the resistivity per defect is insensitive to the degree of clustering, at least for relatively small clusters and for clusters that occur in neutron-generated cascades.

Also deserving consideration is whether the analysis based on Eq. (1) remains valid in spite of the macroscopic inhomogeneity of the defect distribution (i.e., the variation of the defect density with depth inside the film). This question is discussed in the final paragraph of Sec. IV; we conclude there that the detailed damage distribution need not be accounted for explicitly in our analysis and that Eq. (1) is adequate.

III. THEORETICAL ANALYSIS

For comparison with experimental values of ν [cf. Eq. (1)], theoretical calculations of damage production were performed. For simplicity, it was assumed that random collisions occur between the projectile and target atoms. The damage produced by individual target-atom recoils was represented by a modified Kinchin-Pease damage function. In part A, an equation is derived that relates ν to the differential scattering cross section, the stopping power, and the damage function. The forms of these three functions employed in numerical computations are described in part B. The primary recoil spectrum is discussed in part C. Finally, in part D the question of losses to the front and back surfaces in thin-film experiments is considered.

A. Damage-production calculation

Assuming an amorphous target, Lindhard et al.[23] derived an integrodifferential equation that governs the damage energy deposited by an incident ion. The damage energy, as usual, denotes the incident-ion energy minus the energy dissipated in electronic excitations. If $\mathscr{E}_p(E)$ is the damage energy associated with a projectile of energy E and $\mathscr{E}_t(T)$ is the damage energy associated with a target atom recoil of energy T, the equation referred to above may be written

$$\int d\sigma \left[\mathscr{E}_p(E-T) + \mathscr{E}_t(T) - \mathscr{E}_p(E)\right] - S_e(E)\frac{d\mathscr{E}_p}{dE} = 0 ,$$

(3)

where $d\sigma$ is the differential of the projectile-target scattering cross section, and $S_e(E)$ is the projectile-target electronic-stopping cross section (the stopping power dE/dx is equal to $nS_e(E)$, where n is the atomic density of the target). It is assumed in deriving Eq. (3) that no correlation exists between electronic and nuclear stopping processes, and atomic binding effects are neglected. This equation is subject to the boundary condition

$$\lim_{E\to 0} \mathscr{E}(E)/E = 1 .$$

If a solution to Eq. (3) is known for the case of self-ions $(p=t)$, then a useful approximation is available for calculating $\mathscr{E}_p(E)$ for any projectile. Lindhard et al.[23] obtained numerical solutions of Eq. (3) for $p=t$ based on Thomas-Fermi cross sections and velocity-proportional electronic stopping. Their results can be cast in the approximate form

$$\mathscr{E}_t(E) = E/[1 + kg(\epsilon)] ,$$

(4)

where ϵ and k are defined in Sec. IIIB and[24]

$$g(\epsilon) = 3.4008\epsilon^{1/6} + 0.40244\epsilon^{3/4} + \epsilon .$$

(5)

A considerable simplification occurs if the first-order expansion

$$\mathscr{E}_p(E-T) \simeq \mathscr{E}_p(E) - T\frac{d\mathscr{E}_p(E)}{dE}$$

(6)

is substituted into Eq. (3). One then obtains

$$\left[\int T \, d\sigma + S_e(E) \right] \frac{d\mathcal{E}_p(E)}{dE} = \int d\sigma \, \mathcal{E}_t(T). \tag{7}$$

Recognizing that

$$\int T \, d\sigma = S_n(E), \tag{8}$$

the nuclear stopping cross section, we can rearrange Eq. (7) to read

$$\mathcal{E}_p(E) = \int \frac{dE'}{S(E')} \int dT \, \frac{d\sigma(E', T)}{dT} \, \mathcal{E}_t(T), \tag{9}$$

where $S(E) = S_n(E) + S_e(E)$ is the total stopping cross section. Equation (9) in conjunction with Eq. (4) enables one to calculate the damage energy for any projectile-target combination by straightforward numerical integration, assuming the scattering cross section and the stopping power are known.

The approximation in Eq. (6) should be reasonably accurate in the present context, since the scattering cross section $d\sigma/dT$ is weighted toward low-energy recoils. Calculations of the damage energy by the use of Eq. (9) are in excellent agreement with the results of Winterbon.[25]

An equation identical to Eq. (3), apart from the boundary condition, applies to the number of Frenkel pairs $\nu_p(E)$ produced by an incident projectile

$$\int d\sigma \left[\nu_p(E - T) + \nu_t(T) - \nu_p(E) \right] - S_e(E) \frac{d\nu_p(E)}{dE} = 0. \tag{10}$$

Adopting an approximation exactly analogous to Eq. (6) and substituting into Eq. (10), we obtain

$$\nu_p(E) = \int \frac{dE'}{S(E')} \int dT \, \frac{d\sigma(E', T)}{dT} \, \nu_t(T). \tag{11}$$

Equation (11) has been employed in the present numerical calculations of defect production. The damage function $\nu_t(T)$ was represented by the modified Kinchin-Pease expression[26,27]

$$\nu_t(T) = \begin{cases} 0, & T < E_d \\ 1, & E_d \lesssim T < 2.5E_d \\ 0.8\mathcal{E}(T)/2E_d, & T > 2.5E_d, \end{cases} \tag{12}$$

where E_d is an effective displacement threshold energy. We have adopted the displacement threshold energies recommended by Lucasson[19] on the basis of electron-irradiation studies.

In reality, the threshold energy in a crystal is anisotropic, and typically defect production is easiest for recoils near close-packed directions.[19] If

$\nu_t(T)$ is averaged over all crystallographic directions, the resultant function $\langle \nu_t(T) \rangle$ is expected to rise gradually, starting at a minimum threshold energy, rather than discontinuously as in Eq. (12). Equation (12) is based on the hypothesis that the true damage function $\langle \nu(T) \rangle$ can be replaced by a step function, if an appropriate average threshold energy E_d is chosen. Lucasson[19] suggests a value of E_d equal to 1.4 times the minimum threshold energy in the case of an fcc crystal.

The similarity between Eqs. (3) and (10) implies that $\nu_t(T) \propto \mathcal{E}(T)$ at high recoil energies $(T \gg E_d)$. In general, the proportionality constant depends on the interatomic potential; the present choice (0.8/$2E_d$) has been found[26,27] to be appropriate for Thomas-Fermi interactions.

It is worth noting that Eq. (11) can be easily understood on intuitive grounds. The integral in Eq. (11) may be viewed as a sum of the defects produced in each path-length segment $dE/S(E)$ along the range of the projectile. It is clear from this interpretation that such a formulation can be correct only if low-energy recoils dominate [cf. Eq. (6)], since otherwise the differential path length could not be accurately represented as $dE/S(E)$.

The phenomenon of channeling is not included in the present formulation. Some attempts have been made to include channeling in analytical models of damage production, but these do not seem realistic.[28] Binary collision calculations[29,30] indicate that, at least in the case of self-ions, channeling plays an insignificant role in the damage production.

B. Projectile-target interaction and damage function

To evaluate the integrals in Eqs. (9) and (11) explicitly, the stopping power and the scattering cross section must be known. We have adopted the differential scattering cross section based on the Thomas-Fermi potential as formulated by Lindhard et al.[31] (cf. Latta and Scanlon,[32])

$$\frac{d\sigma}{dT} = \frac{\pi a^2 \beta E}{2} \frac{\mathcal{F}_L(t^{1/2})}{t^{3/2}}. \tag{13}$$

Here $a = 0.8853 a_0/(Z_1^{2/3} + Z_2^{2/3})^{1/2}$, where a_0 is the Bohr radius, and Z_1 and Z_2 are the atomic numbers of the projectile and target, respectively; $\beta = a^2 M_2/4M_1 Z_1^2 Z_2^2 e^4$, where M_1 and M_2 are the atomic masses and e is the electronic charge; $t = \epsilon^2 T/T_m$, where $T_m = 4M_1 M_2 E/(M_1 + M_2)^2 \equiv \gamma E$ is the maximum recoil energy, and $\epsilon = a M_2 E/(M_1 + M_2) Z_1 Z_2 e^2$. The function $\mathcal{F}_L(t^{1/2})$ is tabulated numerically in Ref. 31.

It is normally assumed that the Thomas-Fermi potential adequately represents the interatomic forces for most radiation-damage applications.
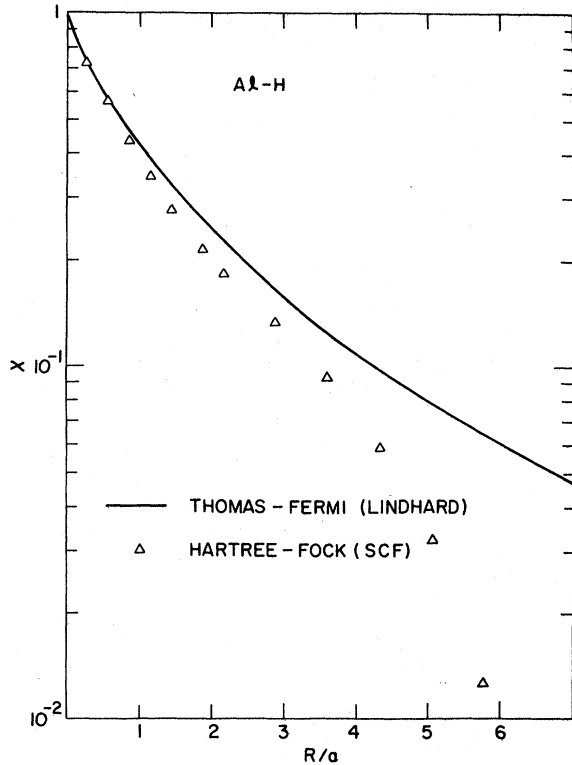
FIG. 1. Screening function $\chi = \Phi(R)R/Z_1Z_2e^2$ for Al-H based on (a) Thomas-Fermi potential with Lindhard screening length and (b) molecular Hartree-Fock calculation. Potentials are in good agreement for $R \lesssim a$.

In some cases, more sophisticated calculations of interatomic potentials have been performed. In Fig. 1, the screening function for Al-H obtained from a Hartree-Fock self-consistent-field calculation[33] may be compared with the Thomas-Fermi screening function $\chi(R/a)$. In the case of energetic protons incident on Al, the minimum energy required to produce Frenkel pairs is ~120 eV, which corresponds to $\chi \sim 0.25$. It can be seen that, for energies in this range and above, the agreement between the Thomas-Fermi potential and the Hartree-Fock potential is reasonably good.

Wilson *et al.*[34] have calculated interatomic potentials for a variety of systems based on a local density approach in which Hartree-Fock-Slater rather than statistical charge densities are employed. Their results show negative deviations from the Thomas-Fermi screening function at large separations, similar to those that appear in Fig. 1. They have derived a function $\mathcal{F}_W(t^{1/2})$, to be used in conjunction with Eq. (13), that represents, in an average way, scattering associated with their calculated interatomic potentials. The functions $\mathcal{F}_W$ and $\mathcal{F}_L$ are in good agreement except at low t. The use of $\mathcal{F}_W$ rather than $\mathcal{F}_L$ in Eq. (11)

resulted in a ~5%-10% lower calculated damage production for the present irradiations.

We turn now to a discussion of the stopping powers. The nuclear stopping cross section $S_n(E)$ may be calculated from Eqs. (13) and (8). One obtains

$$S_n(E) = (\pi a^2 T_m/\epsilon)s_n(\epsilon) , \qquad (14)$$

where

$$s_n(\epsilon) = \frac{1}{\epsilon}\int_0^\epsilon \mathcal{F}_L(\zeta)\,d\zeta .$$

The function $s_n(\epsilon)$ is tabulated in Ref. 31. The electronic stopping power is not well established in the energy range of the present experiments (~0.01 MeV/nucleon). At somewhat higher energies a semiempirical interpolation scheme based on the concept of effective charge has proven useful.[35] At low energies, the theory of Lindhard and Scharff[36] gives a velocity-proportional stopping power

$$S_e = \xi_e 8\pi e^2 a_0 (Z_1 Z_2/Z)v/v_0 , \qquad (15)$$

where

$$Z^{2/3} = Z_1^{2/3} + Z_2^{2/3}, \quad \xi_e \approx Z_1^{1/6}$$

and v_0 is the Bohr velocity. Equation (15) is often recast in the dimensionless form

$$s_e = -\frac{d\epsilon}{d\rho} = k\epsilon^{1/2} ,$$

where

$$k = \frac{0.0793 Z_1^{2/3} Z_2^{1/2}(M_1 + M_2)^{3/2}}{(Z_1^{2/3} + Z_2^{2/3})^{3/4} M_1^{3/2} M_2^{1/2}}$$

and

$$\rho = xn\pi a^2 \gamma .$$

Here x represents length and ρ is a dimensionless reduced length. Starting from a different physical model, Firsov[37] has derived a similar expression but with a slightly different proportionality constant k. Neither the Lindhard-Scharff nor the Firsov theories predicts the existence of Z_1 oscillations, which are observed experimentally. The latter phenomenon is basically an atomic size effect.[38,39] Low-energy stopping measurements for both amorphous carbon[40] and gold[41] targets have been fit to the form

$$S_e = KE^p ,$$

where K and p are constants (for a particular projectile-target combination). The exponent p is an oscillatory function of Z_1 for a given target. Its value is, in some cases, considerably different from $\frac{1}{2}$.

Unfortunately, extensive stopping data of the type mentioned above[40,41] is not available for cop-

per and silver targets. In the absence of such data, we have employed the Lindhard-Scharff stopping formula and the semiempirical stopping power tables of Northcliffe and Schilling[42] in the present numerical calculations. The calculations of defect production based on Eq. (11) are most sensitive to the electronic stopping power in the case of the light ions, for which nearly all of the incident energy is dissipated in electronic excitations.

Finally, some remarks are appropriate concerning the remaining factor $\nu_t(T)$ on the right-hand side of Eq. (11). The modified Kinchin-Pease expression given in Eq. (12) should be regarded as a zero-order model rather than an attempt to represent the exact damage function, which is certainly more complicated. The primary objective of the present study is to establish the actual form of $\nu_t(T)$. In Sec. IV, the damage rates determined in ion-irradiation experiments are expressed in terms of a production "efficiency"

$$\xi = \nu^e(E)/\nu_p(E), \tag{16}$$

where ν^e is calculated from Eq. (1) and $\nu_p(E)$ is the theoretical value obtained from Eq. (11). Deviations of this efficiency from unity will be discussed in the light of possible inadequacies of the modified Kinchin-Pease damage function.

C. Primary recoil spectrum

Ion irradiations at different energies and/or different projectile species can be compared in terms of the spectra of recoil energies. The number of recoils produced between energies T and $T + dT$ is proportional to

$$P(T)dT = \frac{1}{N_R} \int \frac{dE}{S(E)} \frac{d\sigma(E,T)}{dT} dT,$$

where the normalization constant is given by

$$N_R = \int \frac{dE}{S(E)} \int_{E_d}^{\gamma E} \frac{d\sigma(E,T)}{dT} dT.$$

In Fig. 2, recoil spectra $\Pi(T) = TP(T)$ are plotted for four of the irradiations performed in the present work. One notes an enormous shift in the spectra as the mass and energy of the projectile are increased. It is also of some interest to consider the number of defects generated as a function of recoil energy. In Fig. 3, we have plotted the fraction of defects η produced in all recoils of energy below T',

$$\eta(T') = \frac{1}{\nu_p(E)} \int_{E_d}^{T'} P(T)\nu_t(T) dT \tag{17}$$

for the irradiations treated in Fig. 2.

The primary recoil spectrum may be employed to calculate various averages. For example, the average energy is given by

$$\langle T \rangle = \int P(T)T \, dT.$$

H→Ag 20 keV ——————
He→Ag 40 keV — — — —
O→Ag 150 keV —·—·—
Bi→Ag 720 keV ·········
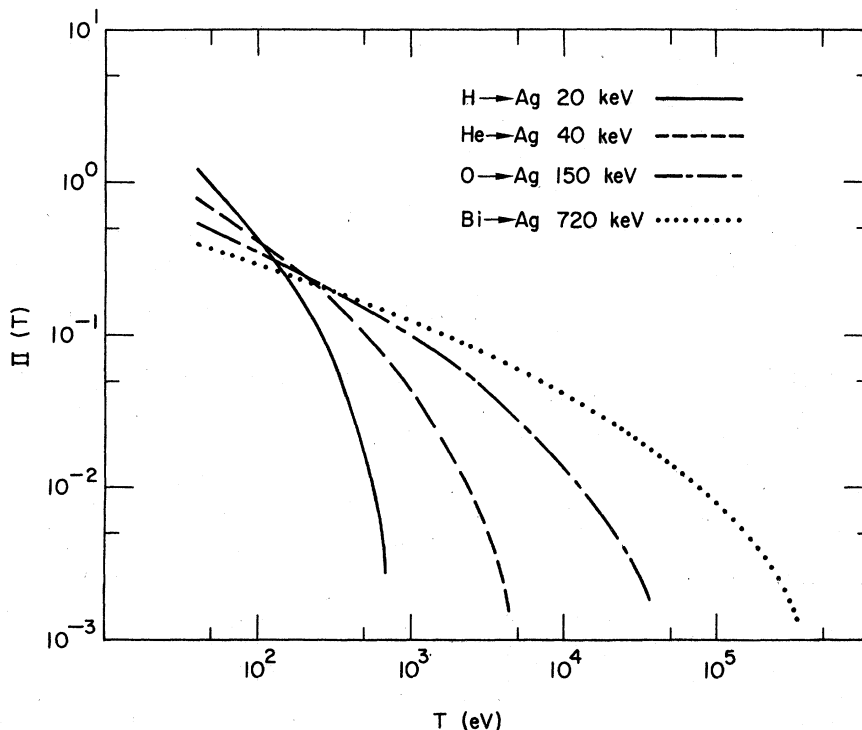
FIG. 2. Primary recoil spectrum $\Pi = TP(T)$ calculated for several types of radiation employed in the present experiments. The change in the particle mass is mainly responsible for the shifts in the recoil spectrum.
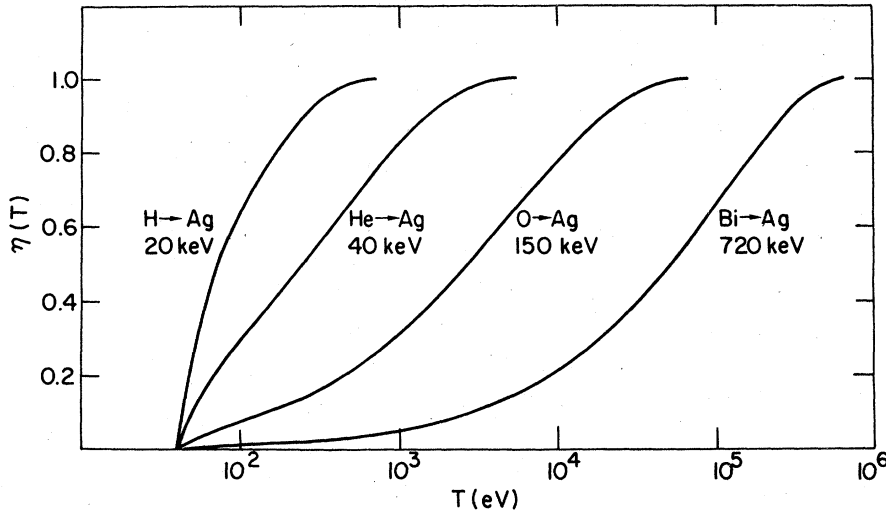
FIG. 3. Fraction of defects produced in cascades initiated by recoils of energy below T. Calculations for four types of irradiation are shown.

Another parameter of interest, which we refer to as the "weighted-average" recoil energy, is given by

$$\langle T_w \rangle = \frac{1}{\nu_p(E)} \int P(T)\nu_t(T)T dT . \tag{18}$$

The quantity $\langle T_w \rangle$ is somewhat greater than $\langle T \rangle$, since, in Eq. (18) recoils are weighted by the damage function $\nu_t(T)$, which increases with energy.

Unfortunately, the recoil spectrum cannot be fully characterized by a single parameter, such as $\langle T \rangle$ or $\langle T_w \rangle$. However, these parameters do give a measure of the hardness of a given recoil spectrum. One can argue that $\langle T_w \rangle$ is more significant than $\langle T \rangle$, since physically observable quantities depend on the number of defects produced and high-energy recoils create more defects than those at low energy. In Sec. IV, the variation of efficiency ξ as a function of weighted-average recoil energy $\langle T_w \rangle$ is discussed.

D. Surface losses

The random-collision calculations described thus far apply to an infinite solid. Ion-damage experiments, however, are generally performed on thin-film specimens. We consider now to what extent the present experimental results are affected by losses to the specimen surfaces. This problem can be addressed theoretically by transport calculations of the depth distribution of energy deposition.[25,43] Such calculations permit the estimation of energy reflection at the front surface and energy transmission through the back surface. In the energy range of the present experiments ($\epsilon \sim 1$–5) the losses by both transmission and reflection are substantial only for light-ion irradiation. The losses

by reflection, in the case of 20-keV-proton irradiation of Ag, are <10%, according to the transport calculations by Weissmann and Sigmund[44] and the Monte Carlo computer simulations by Robinson and Agamy.[45] The energy reflection is considerably smaller for heavy ions. Considering a wide range of projectile-target combinations, Winterbon[25] calculates sputtering efficiencies of only a few percent in the energy range of the present work. Measured reflection coefficients by Bottiger et al.[46] are in reasonable agreement with the predictions of transport theory.

Losses by transmission may also be considerable for light ions because of the pronounced range straggling for such irradiation. Figure 4 shows damage energy profiles for 40-keV He and 950-keV Ag ions incident on an Ag target. The curves were obtained by scaling drawings given in the monograph of Winterbon[25] to the appropriate projected range, which is ~1400 Å in both cases. One observes that the damage energy straggling is much greater for He than for Ag irradiations, although the peak positions are approximately the same. For a film of thickness $t = 2800$ Å, integration of the area under the curve for $x > t$ indicates that <10% of the beam energy for 40-keV He is lost by transmission.

We estimate that, for the present experiments, surface losses are at worst of the order of 10%–20% for the light ions and are considerably less for the heavy ions.

IV. RESULTS

Results of irradiations on Ag and Cu targets are given in Tables I and II, respectively. As mentioned earlier, the energy for the majority of the
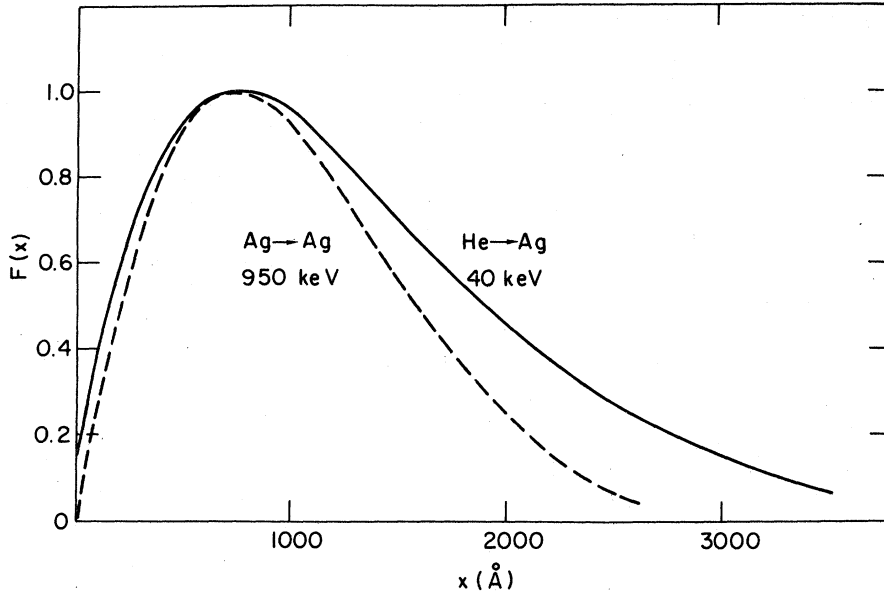
FIG. 4. Damage-depth distributions for two types of irradiation. Although the mean projected ranges are essentially the same, losses to both the front and back surfaces (at $x = 2800$ Å, say) are greater for the light-particle irradiation. Curves are based on figures given in Winterbon's monograph.

irradiations was chosen such that $\langle R_p \rangle \sim \frac{1}{2}t$. In the case of some of the heavy projectiles, however, the maximum energy available on our accelerator corresponded to a lower projected range. The projected range $\langle R_p \rangle$ was estimated from interpolation formulas proposed by Schiott.[47] The resistivity damage rates $d\Delta\rho/d\phi$ that appear in the tables have been corrected for both size effect and radiation annealing, as described in Sec. II. Equation (1) was employed to calculate ν_p^e, the number of Frenkel pairs per incident ion. Damage efficiencies that correspond to the Lindhard-Scharff stopping formula and to the Northcliffe-Schilling stopping power tables are denoted ξ^L and ξ^{NS}, respectively. These quantities are calculated on the basis of Eqs. (11), (12) and the values of ν_p^e given in the tables. The uncertainty in the thickness determination is ~10% for most specimens. For specimen nos. 2 and 3, special care was taken to determine the thicknesses to an accuracy of ≤5%. It is seen that agreement between results for these specimens is quite good, although the thicknesses differ considerably.

Efficiency is plotted versus weighted-average recoil energy $\langle T_w \rangle$ for Ag and Cu in Figs. 5 and 6. The curves in these figures correspond to the data in Tables I and II, respectively. In those cases in which data are given for more than one specimen, the average value is plotted. One observes similar trends for both metals; ξ decreases monotonically as $\langle T_w \rangle$ increases and approaches an apparent plateau at high $\langle T_w \rangle$. It was noted in Sec. III, that in the case of light ions, the calculated damage rates $\nu_p(E)$ are sensitive to the electronic stopping power. This feature is reflected in the relatively large

values of the difference $\xi^{NS} - \xi^L$ that occur for the light-ion irradiations. Nevertheless, the trend of decreasing efficiency with increasing $\langle T_w \rangle$ is observed regardless of the particular stopping-power model that is employed.

It is interesting to compare the efficiencies for light ions that are stopped within the specimen with those obtained in transmission experiments.[11] The analysis of the latter type of experiment is insensitive to the assumed stopping power. The bottom entries in Tables I and II correspond to ion transmission. One can see that the efficiencies for stopped and transmitted H and He ions are in rough agreement despite possible errors in the assumed stopping powers.

As discussed in Sec. III, no single parameter such as $\langle T_w \rangle$ completely characterizes the recoil spectrum. We have selected $\langle T_w \rangle$ as a convenient scale by which to compare the results of different irradiations, e.g., in Figs. 5 and 6. However, one may equally well correlate efficiency with other parameters. In Tables I and II, values are given for (a) the recoil energy $T_{1/2}$ below which half the defects are produced $[\eta(T_{1/2}) = 0.5]$, (b) the maximum stopping power S_n^*, calculated from Eq. (14), and (c) the fraction of defects produced below $\tilde{T} = 2$ keV. ($\tilde{T}$ was identified in Ref. 11 as the approximate energy at which a transition occurs from high efficiency to low efficiency in Ag.) All of these quantities are correlated to the efficiency.

For certain projectiles, damage rates have been measured as a function of energy. The "apparent" energy dependence of efficiencies obtained for He irradiations of Ag are plotted in Fig. 7. For energies above ~60 keV, a considerable fraction of the

TABLE I. Damage data for ion irradiations of silver.

Specimen[a]	Projectile	E (keV)	$d\Delta\rho/d\phi$ (Ω cm³)	ν^e	ξ^L	ξ^{NS}	$\langle T_w \rangle$ (keV)	$T_{1/2}$ (keV)	η (2 keV)	S_n^* (eV cm²/atom)
1	¹H[b]	20	0.48×10⁻²¹	2.92	0.81	1.05	0.117	0.073	1.00	9.79×10⁻¹⁶
2	¹H	20	0.37×10⁻²¹	2.68	0.74	0.96	0.117	0.073	1.00	⋯
3	¹H	20	0.27×10⁻²¹	2.86	0.79	1.02	0.117	0.073	1.00	⋯
4	¹H	25	0.23×10⁻²¹	3.02	0.75	0.97	0.130	0.077	1.00	⋯
5	¹H	20	0.47×10⁻²¹	2.86	0.79	1.03	0.117	0.073	1.00	⋯
5	²D	20	1.29×10⁻²¹	8.3	0.71	0.90	0.185	0.096	1.00	1.94×10⁻¹⁵
2	²D	15	0.96×10⁻²¹	7.0	0.69	0.87	0.159	0.089	1.00	⋯
5	³He	40	3.29×10⁻²¹	20.2	0.61	0.90	0.441	0.201	0.96	5.65×10⁻¹⁵
5	⁴He	40	4.38×10⁻²¹	26.9	0.56	0.81	0.570	0.250	0.94	7.47×10⁻¹⁵
6	⁴He	35	4.00×10⁻²¹	30.9	0.68	0.98	0.525	0.238	0.95	⋯
4	⁴He	65	2.53×10⁻²¹	32.4	0.55	0.80	0.759	0.294	0.89	⋯
2	⁴He	40	3.89×10⁻²¹	28.6	0.59	0.86	0.570	0.250	0.94	⋯
3	⁴He	40	2.77×10⁻²¹	29.9	0.62	0.90	0.570	0.250	0.94	⋯
6	⁷Li	40	0.72×10⁻²⁰	55.8	0.58	0.81	1.05	0.47	0.83	4.88×10⁻¹⁴
3	⁷Li	40	0.51×10⁻²⁰	55.1	0.58	0.81	1.05	0.47	0.83	4.63×10⁻¹⁴
1	¹¹B	90	1.85×10⁻²⁰	116	0.48	0.64	3.14	1.30	0.60	5.93×10⁻¹⁴
6	¹²C	110	1.73×10⁻²⁰	135	0.45	0.59	4.09	1.69	0.55	5.90×10⁻¹⁴
2	¹²C	100	1.65×10⁻²⁰	121	0.43	0.56	3.91	1.66	0.56	7.85×10⁻¹⁴
6	¹⁴N	150	2.19×10⁻²⁰	170	0.41	0.54	6.04	2.38	0.47	1.00×10⁻¹³
6	¹⁶O	150	2.33×10⁻²⁰	182	0.39	0.49	7.08	2.89	0.43	1.49×10⁻¹³
6	²⁰Ne	200	3.43×10⁻²⁰	266	0.395	0.46	11.09	4.52	0.35	3.75×10⁻¹³
6	³⁵Cl	260	0.62×10⁻¹⁹	477	0.40	0.42	23.20	10.22	0.23	4.36×10⁻¹³
6	⁴⁰Ar	300	0.68×10⁻¹⁹	530	0.375	0.40	28.37	12.41	0.20	⋯
2	⁴⁰Ar	300	0.66×10⁻¹⁹	486	0.345	0.37	28.37	12.41	0.20	⋯
3	⁴⁰Ar	360	0.55×10⁻¹⁹	594	0.370	0.395	32.51	13.79	0.20	⋯
4	⁴⁰Ar	500	5.12×10⁻²⁰	656	0.33	0.35	40.55	15.97	0.18	⋯
6	⁵⁶Fe	260	0.74×10⁻¹⁹	575	0.39	0.39	32.53	15.48	0.17	7.60×10⁻¹³
6	¹⁰⁷Ag	540	1.67×10⁻¹⁹	1289	0.40	0.39	77.34	39.22	0.10	1.83×10⁻¹²
1	²⁰⁹Bi	720	2.16×10⁻¹⁹	1533	0.33	0.32	101.5	53.80	0.08	3.86×10⁻¹²
					Transmission					
⋯	¹H	150	0.90×10⁻²²	⋯	⋯	0.91	0.869	0.337	0.85	⋯
⋯	⁴He	290	0.75×10⁻²¹	⋯	⋯	0.73	4.670	1.300	0.57	⋯

[a] Specimen thicknesses are for no. 1, 2.30×10⁻⁵ cm; for no. 4, 4.60×10⁻⁵ cm; for no. 5, 2.20×10⁻⁵ cm; for no. 6, 2.78×10⁻⁵ cm; and for no. 3, 3.88×10⁻⁵ cm. Specimens 1 and 4 are single crystals. Specimens 5, 6, 2, and 3 are polycrystalline.

[b] Damage rates corrected for the resistivity of H or D, which is assumed to be 1.5×10⁻⁶ Ω cm/at.%.

TABLE II. Damage data for ion irradiations of copper.

Specimen	Projectile	E (keV)	$d\Delta\rho/d\phi$ (Ω cm^3)	ν^e	ξ^L	ξ^{NS}	$<T_w>$ (keV)	$T_{1/2}$ (keV)	η (2 keV)	S_n^* (eV cm^2/atom)
7	^{1}H^b	17	0.52×10^{-21}	6.8	1.18	1.21	0.123	0.065	1.00	1.18×10^{-15}
8	^{4}He	35	0.55×10^{-20}	58	0.89	1.05	0.680	0.265	0.90	9.06×10^{-15}
8	^{7}Li	54	1.15×10^{-20}	122	0.78	0.93	1.67	0.636	0.74	1.88×10^{-14}
8	^{12}C	100	2.13×10^{-20}	226	0.58	0.67	4.91	1.81	0.53	6.58×10^{-14}
8	^{14}N	115	2.46×10^{-20}	262	0.54	0.62	6.38	2.43	0.47	8.60×10^{-14}
8	^{16}O	130	2.86×10^{-20}	304	0.52	0.58	7.99	3.03	0.42	1.08×10^{-13}
8	^{22}Ne	160	3.78×10^{-20}	400	0.48	0.51	12.28	4.92	0.34	1.69×10^{-13}
8	^{40}Ar	320	0.71×10^{-17}	750	0.39	0.39	31.82	12.69	0.21	4.24×10^{-13}
8	^{56}Fe	270	0.62×10^{-19}	658	0.34	0.33	33.87	15.45	0.18	6.89×10^{-13}
9	^{63}Cu	500	1.09×10^{-19}	1143	0.34	0.34	56.03	23.54	0.15	8.18×10^{-13}
8	^{86}Kr	520	1.29×10^{-19}	1373	0.36	0.35	62.31	27.13	0.13	1.12×10^{-12}
9	^{107}Ag	560	1.46×10^{-19}	1535	0.36	0.34	68.78	32.54	0.12	1.53×10^{-12}
9	^{209}Bi	855	2.41×10^{-19}	2539	0.37	0.36	88.54	44.89	0.095	2.94×10^{-12}
					Transmission					
$\cdots$	H	150	0.75×10^{-22}	$\cdots$	$\cdots$	0.78	1.191	0.335	0.80	$\cdots$
8	He	260	0.64×10^{-21}	$\cdots$	$\cdots$	0.60	5.740	1.216	0.57	$\cdots$

^{a}Specimen thicknesses are: for no. 9, 2.48×10^{-5} cm, for no. 8, 2.50×10^{-5} cm, and for no. 7, 3.10×10^{-5}cm. All specimens are polycrystalline.

^{b}Damage rate corrected for resistivity of H, which is assumed to be $1.5\times10^{-6}/\Omega$ cm/at.% [W. R. Wampler], T. Schober, and B. Lengeler, Philos. Mag. **34**, 129 (1976)].

beam energy is transmitted through the back surface of the specimen, which was 2800 Å thick. For energies below this value, the energy dependence of the efficiencies is roughly consistent with the slope of the curve in Fig. 5 at equivalent values of $\langle T_w \rangle$. The open circles represent efficiencies corrected for losses to the back surface. The correction factors were obtained from damage-energy-distribution curves generated by the RASE3 and DAMG2 codes developed by Brice.[48] In the latter calculations, the electronic stopping was represented by the Lindhard-Scharff formula.

Efficiencies obtained for Ne and Ar irradiations of Ag at several energies are given in Table III. One observes that the efficiencies are nearly constant. In the energy range considered, losses to the back surface are negligible. The relatively constant efficiencies for Ne and Ar are consistent with the results in Fig. 5, since only small intervals in $\langle T_w \rangle$ are spanned at the irradiation energies listed in Table III.

The energy dependence of damage rates can be used to calculate approximate stopping powers, provided losses to the surfaces can be ignored. Differentiating Eq. (11) with respect to E and substituting Eq. (16), we obtain

$$\frac{dv_p^e}{dE} = \frac{\sigma(E)}{S(E)}\xi(E),\qquad(19)$$

where

$$\sigma(E)=\int_{E_d}^{\gamma E}\frac{d\sigma}{dT}v_t(T)\,dT.$$

Decomposing the stopping power into electronic and nuclear components $S = S_n + S_e$, we can rewrite Eq. (19) in the form

$$S_e(E) = \frac{\sigma(E)\xi(E)}{dv_p^e/dE} - S_n(E).\qquad(20)$$

The quantity dv_p^e/dE can be calculated by differentiating Eq. (1) and using the energy dependence of
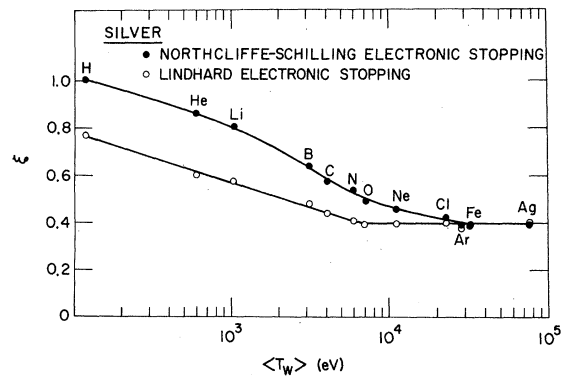
FIG. 5. Efficiencies obtained for ion irradiations of Ag, based on Lindhard-Scharff electronic stopping and on Northcliffe-Schilling electronic stopping. Ion energies are given in Table I. In cases in which more than one measurement is listed in the Table, the average value is plotted.
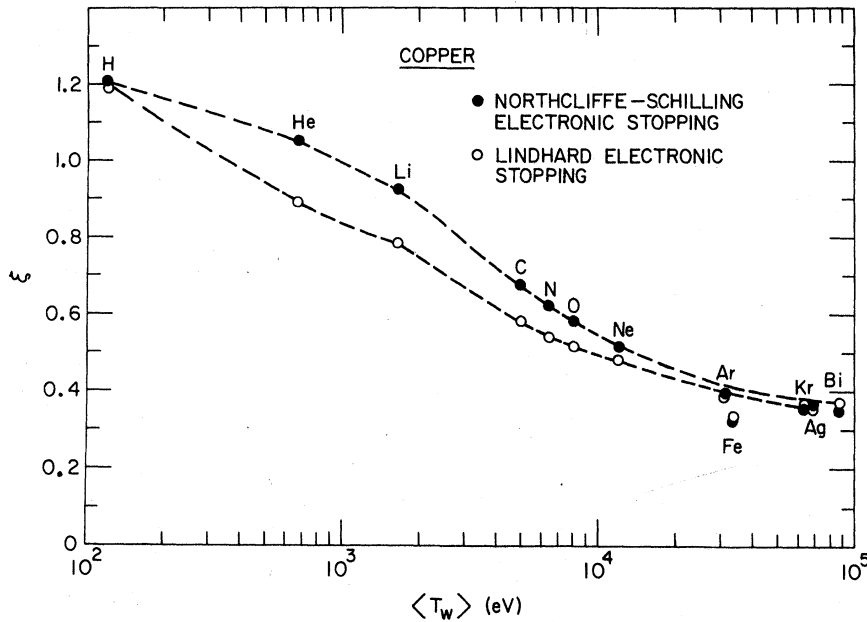
FIG. 6. Efficiencies obtained for ion irradiations of Cu based on Lindhard-Scharff electronic stopping and on Northcliffe-Schilling electronic stopping. Ion energies are given in Table II. Values plotted correspond to specimens 7, 8, and 9.

experimental damage rates. The efficiency $\xi(E)$ corresponds in principle to the irradiation of a film of infinitesimal thickness. If a value for this parameter is known and S_n is calculated from Eq. (14), then Eq. (20) can be evaluated to obtain the electronic stopping power. This procedure was employed to analyze the results for Ne and Ar irradiations of Ag. Values of S_e calculated from Eq.

(20) were of the same order of magnitude as those given by Eq. (15) and the Northcliffe-Schilling tables. However, the present stopping powers show a somewhat more rapid energy dependence $(p > \frac{1}{2})$ than the usual velocity-porportional forms. A more complete report on the above stopping-power analyses will be given elsewhere.

We return now to the question raised at the con-
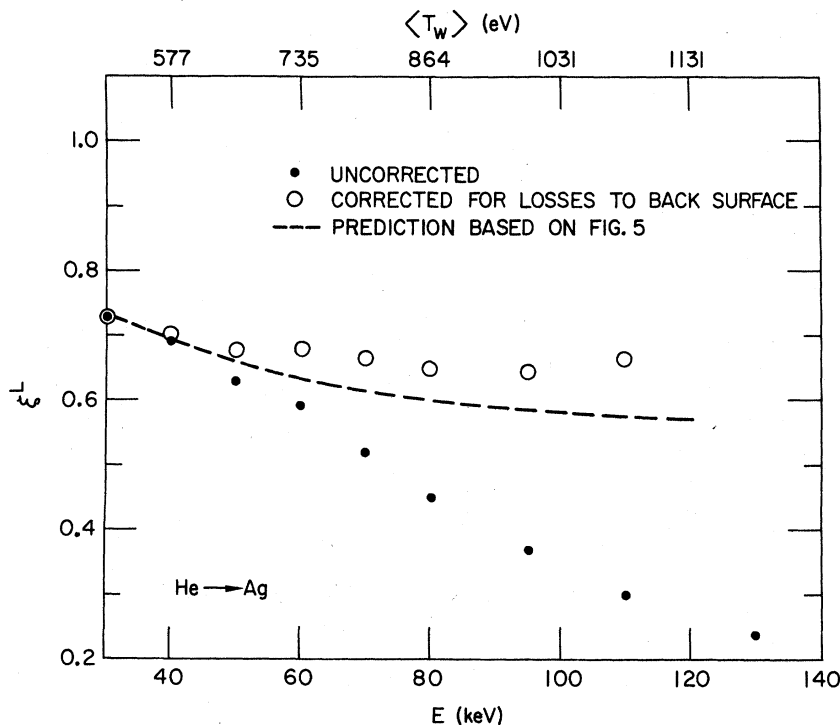
FIG. 7. Efficiency as a function of energy for He irradiation on a 2800-Å Ag target. The Lindhard electronic stopping function is employed. The closed circles show the results uncorrected for losses to the back surface. The open circles show efficiencies corrected for back-surface losses on the basis of depth-distribution curves generated by the Brice code, DAMG2.

TABLE III. Energy dependence of the damage efficiency for neon and argon irradiation of silver.

					Ar					
Energy (keV)	140	160	180	200	240	280	320	360	400	460
ξ^L	0.32	0.35	0.34	0.35	0.355	0.37	0.38	0.36	0.35	0.365
					Ne					
Energy (keV)	100	150	175	200	225	250	275			
ξ^L	0.385	0.39	0.40	0.39	0.40	0.395	0.40			

clusion of Sec. II, i.e., whether the analysis based on Eq. (1) is valid in the presence of nonhomogeneous defect distributions such as those exhibited in Fig. 4. In this regard, it is important to bear in mind that the electronic mean free path is greater than the film thickness. Accordingly, the electrical resistivity increment $\Delta\rho$ is expected to be proportional to the total number of scattering centers (i.e., defects) but insensitive to their arrangement on a scale finer than the mean free path. The following observations tend to confirm this expectation: (a) The Frenkel pair production ν^e deduced from Eq. (1) was found essentially independent of the specimen thickness (cf. Table I). (b) The efficiencies for Ar and Ne irradiation of Ag were nearly constant as a function of energy over a wide energy interval (cf. Table III). When the projectile energy is varied, the damage distribution changes correspondingly; if the analysis were extremely sensitive to the damage distribution one would expect a large variation in the efficiency as a function of energy, contrary to the results shown in Table III. (c) The efficiencies calculated from Eq. (1) were found to be insensitive to the sequence of projectiles selected for irradiation of a given specimen. Thus the efficiency determined for a given projectile and energy was essentially independent of the previous history of the specimen. For all of these reasons, we believe that inhomogeneity in the damage distribution does not strongly influence our results and need not be taken into account explicitly in the analysis. There may indeed be certain limiting cases in which the inhomogeneity would have greater importance, for example, if the damaged region were confined to a thin layer close to the surface. We note that the efficiencies for the series of Ar irradiations of Ag at energies 160–460 keV were $\xi = 0.360 \pm 0.02$, i.e., $\pm 5\%$ (cf. Table III), whereas the efficiency for the 140-keV irradiation was 12% lower than the mean. It is possible that this low value is a result of damage inhomogeneity since $\langle R_p \rangle$ is only $\approx 0.2t$ in this case. For all of the irradiations listed in Tables I and II, $\langle R_p \rangle$ is considerably greater than 20% of the specimen thickness.

V. DISCUSSION

The present technique permits damage efficiencies that correspond to a wide variety of recoil spectra to be determined within the framework of a single experiment. As the projectile mass increases (while the energy is adjusted to keep $\langle R_p \rangle$ constant), the recoil spectrum is shifted to higher energies, as reflected, for example in values of $\langle T_w \rangle$ given in Tables I and II. The main objective of the present work was to determine the effect of this recoil-spectrum shift on the defect-production efficiency.

It has been known for some time that the defect-production efficiency associated with high-energy recoils produced, for example, by fast-neutron irradiation is lower than that for recoils near the threshold.[19] However, the behavior of the efficiency between these two extremes as well as the underlying physical mechanisms is not well understood. The present experiments span the range between quite soft and extremely hard spectra and therefore shed some light on this behavior.

We consider first the limit of low $\langle T_w \rangle$. The decrease in efficiency with an increase in $\langle T_w \rangle$ in this limit (cf. Figs. 5 and 6) indicates that the damage function given in Eq. (12) increases too rapidly at low T. Table IV gives the ratio of the number of defects $\nu_p^e(E)$ to the calculated number of recoils above threshold $N_R(E)$ for light-ion irradiations of Ag. One observes that this ratio is close to unity and almost the same for the He as for the H irradiations. This indicates that the proportion of multiple-displacement events does not increase as rapidly with $\langle T_w \rangle$ as predicted from the model based on Eq. (12). Therefore, a damage function that rises more gradually at low energy would be more realisitc than Eq. (12).

Information concerning $\nu_t(T)$ near the threshold energy can also be obtained from both electron irradiation experiments and computer simulation studies. A few attempts have been made to fit $\nu_t(T)$ directly to electron damage data.[49,50] However, such a procedure does not yield a unique damage function, and the results obtained thus far are not

TABLE IV. Damage data for light-ion irradiations of Ag.

Projectile	Energy (keV)	$<T_w>$ [a] (eV)	$T_{1/2}$ [a] (eV)	ν^e	ν^e/N_R [a]	ξ [a]
H	20	120	74	2.86	0.90	0.79
D	20	190	98	8.3	0.93	0.71
^{3}He	40	450	201	20.2	1.04	0.61
^{4}He	40	580	255	26.9	1.04	0.56
^{4}He	30	490	230	25.4	1.08	0.60

[a] Calculations based on Lindhard-Scharff stopping power.

conclusive. It may be significant, however, that Wollenberger and co-workers[49,50] obtained a damage function for Al that is quite flat at low-recoil energies and begins to increase more rapidly only at ~175 eV, which is more than six times the value of E_d for Al recommended by Lucasson.[19]

The behavior of $\nu_t(T)$ has also been studied by computer simulations of the type developed at Brookhaven.[51-54] Such computations involve the numerical solution of Newton's equations of motion for a crystallite in which one atom is given an initial "knock-on" energy T. A recent dynamical simulation study for Cu has been performed by Schiffgens and Bourquin.[55] They considered twelve crystallographic directions and treated knock-on energies up to 200 eV. The number of stable defects produced at each energy, averaged over direction, are plotted in Fig. 8. The results suggest a damage function that is more complicated than Eq. (12) and has at least two "steps."

We discuss now the efficiency at high $\langle T_w \rangle$. One observes in Figs. 5 and 6 that the efficiency decreases to a limiting value of ~$\frac{1}{3}$ for the heaviest projectiles employed. It is interesting that an apparent plateau occurs in the efficiency for heavy projectiles; very little change in the efficiency is observed for ions heavier than Ne. We shall refer to this behavior as "saturation" of the efficiency. Considering the values of $T_{1/2}$ for the Ne irradiations, it is evident that the limiting efficiency is reached at recoil energies of a few keV.

A satisfactory understanding of the saturation of the efficiency would require an explanation of why the modified Kinchin-Pease model greatly overestimates the defect production for energetic cascades. The latter question has been an outstanding issue for many years. One mechanism that may be relevant will be referred to, loosely, as the thermal spike. According to this concept, recombinations of close Frenkel pairs are induced by agitation in the cascade region following the initial displacement spike. Such recombinations are at least partially responsible for the small amount of stage-I annealing that is associated with cascade damage.[56] The effectiveness of cascade-induced

thermal spikes in the promotion of close-pair recombinations was confirmed in recent radiation-annealing studies.[57] Additional evidence for the thermal-spike mechanism was obtained in a Brookhaven-type dynamical simulation study of a 2.5-keV cascade in W.[58] It was found that two-thirds of the defects observed in a binary-collision simulation (which does not include the thermal spike) of the same cascade are unstable with respect to thermal-spike recombination.

Regardless of whether thermal-spike recombinations are responsible for the low efficiencies observed, it seems likely that the efficiencies are intimately connected with the energy density in cascades. If this is assumed to be the case, the phenomenon of saturation of the efficiency can be plausibly explained in terms of subcascade formation. Thus, the cascades generated by recoils above a certain threshold decompose into more or less distinct regions (subcascades) with higher than average defect density.[59] The higher the recoil energy, the greater the number of subcascades
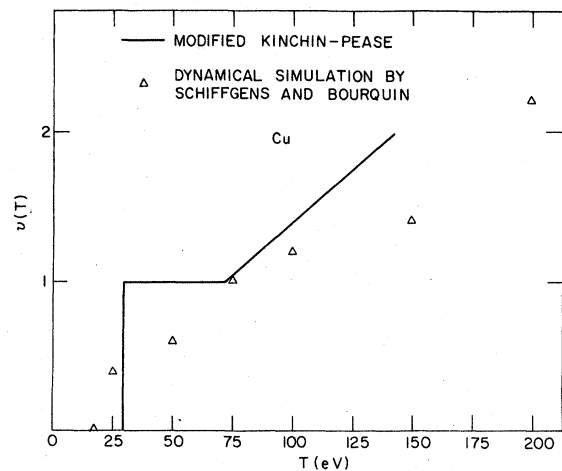
FIG. 8. Modified Kinchin-Pease model employed in the present work is compared with results of recent dynamical simulation studies by Schiffgens and Bourquin. [A slight discontinuity in $\nu(2F_d)$ that occurs in Eq. (12) is not shown.]

generated; however, the energy density and the damage efficiency for each individual subcascade are relatively constant.

According to these considerations, the efficiency for fission fragments, which generate large numbers of subcascades along their tracks, should be comparable to those obtained for heavy ions in the present work. Recent fission-fragment experiments[60] on Cu have yielded an efficiency of ~0.35, in excellent agreement with the results in Fig. 6. One also expects that the efficiencies associated with fission neutrons (which produce recoil energies $T \sim 50$ keV and fusion neutrons ($T \sim 200$ keV) should be similar. This has indeed been found to be the case for several fcc and bcc metals.[61,62]

VI. CONCLUSIONS

The main conclusions to be drawn from the present work are (a) the damage function begins to deviate from the Kinchin-Pease model at recoil energies relatively close to the displacement threshold, and (b) the efficiency apparently saturates for recoil energies above a few keV. The underlying physical mechanism for the deviations from Kinchin-Pease is still not satisfactorily understood. We believe the thermal-spike mechanism to be important in this regard, but other factors may also be involved, particularly at recoil energies near threshold.

The possibility of using the present techniques to study the electronic stopping power has been outlined in Sec. IV and is currently under additional investigation.

ACKNOWLEDGMENTS

[1]M. T. Robinson, in *Fundamental Aspects of Radiation Damage in Metals*, edited by M. T. Robinson and F. W. Young, Jr. (U.S. GPO, Washington, D.C., 1976), Vol. 1, p. 1.

[2]D. M. Parkin and A. N. Goland, Radiat. Eff. 28, 31 (1976).

[3]H. H. Andersen and H. Sorensen, Radiat. Eff. 14, 49 (1972).

[4]K. L. Merkle and L. R. Singer, Appl. Phys. Lett. 11, 35 (1967).

[5]K. Herschbach and J. J. Jackson, Phys. Rev. 153, 689 (1967); 170, 648 (1968).

[6]K. Herschbach, Phys. Rev. 130, 554 (1968).

[7]W. Kohler and W. Schilling, Nukleonik 7, 389 (1965).

[8]H. G. Cooper, J. S. Koehler, and J. W. Marx, Phys. Rev. 97, 599 (1955).

[9]H. T. Coffey, E. L. Keller, A. Paterson, and S. H. Autler, Phys. Rev. 155, 355 (1967).

[10]K. L. Merkle, in Proceedings of the International Conference on Solid State Physics Research with Accelerators, Brookhaven National Laboratory, 1967, Report No. BNL-50083, C52, p. 359 (unpublished).

[11]K. L. Merkle, R. S. Averback, and R. Benedek, Phys. Rev. Lett. 38, 424 (1977).

[12]K. Fuchs, Proc. Camb. Philos. Soc. 34, 100 (1938).

[13]G. Duesing, W. Sassin, W. Schilling, and H. Hemmerich, Cryst. Lattice Defects 1, 55 (1969).

[14]G. Burger, H. Meissner, and W. Schilling, Phys. Status Solidi 4, 281 (1964).

[15]E. H. Sondheimer, Adv. Phys. 1, 1 (1952).

[16]G. Lücke and R. Sizmann, Phys. Status Solidi 5, 683 (1964).

[17]R. C. Birtcher, R. S. Averback, and T. H. Blewitt, J. Nucl. Mater. 75, 167 (1978).

[18]R. S. Averback, K. L. Merkle, and L. J. Thompson, Bull. Am. Phys. Soc. 22, 329 (1976).

[19]See P. Lucasson, in *Fundamental Aspects of Radiation Damage in Metals*, Conf. No. 751006-P1 (U.S. ERDA, Oak Ridge, Tenn., 1976), p. 42.

[20]E. E. Gruber, J. A. Tesk, T. H. Blewitt, and R. E. Black, Phys. Rev. B 2, 2849 (1970).

[21]F. Dworschak, H. Wagner, and P. Wombacher, Phys. Status Solidi 52, 103 (1972).

[22]P. Ehrhart, H. G. Haubold, and W. Schilling, Festkoerperprobleme XIV, 87 (1974).

[23]J. Lindhard, V. Nielsen, M. Scharff, and P. V. Thomsen, Kgl. Dan. Vidensk. Selsk. Mat.-Fys. Medd. 33, 10 (1963).

[24]M. T. Robinson, in *Radiation Induced Voids in Metals*, edited by J. W. Corbett and L. C. Ianiello (U.S.AEC, Oak Ridge, Tenn., 1972), p. 392.

[25]K. B. Winterbon, *Ion Implantation Range and Energy Deposition Distributions* (Plenum, New York, 1975), Vol. 2.

[26]M. J. Norgett, M. T. Robinson, and I. M. Torrens, Nucl. Eng. Design 33, 50 (1974).

[27]P. Sigmund, Radiat. Eff. 1, 15 (1969).

[28]This matter is discussed in M. W. Thompson, *Defects and Radiation Damage in Metals* (Cambridge U. P., London, 1969), p. 183.

[29]J. R. Beeler, Phys. Rev. 150, 470 (1966).

[30]M. T. Robinson and I. M. Torrens, Phys. Rev. B 9, 5008 (1974).

[31]J. Lindhard, V. Nielsen, and M. Scharff, Kgl. Dan. Vidensk, Selsk. Mat.-Fys. Medd. 36, 10 (1968).

[32]B. M. Latta and P. J. Scanlon, Phys. Rev. A 10, 1638 (1974).

[33]N. H. Sabelli, M. L. Kantor, R. Benedek, and T. L. Gilbert, J. Chem. Phys. 68, 2767 (1978).

[34]W. D. Wilson, L. G. Haggmark, and J. P. Biersack, Phys. Rev. B 15, 2458 (1977).

[35]D. Ward, J. S. Forster, H. R. Andrews, I. V. Mitchell, G. C. Ball, W. G. Davis, and G. J. Costa, Atomic Energy of Canada Limited, AECL-5313 (1976); J. F. Ziegler, Appl. Phys. Lett. 31, 544 (1977); B. S. Yarlagadda, J. E. Robinson, and W. Brandt, Phys. Rev. B 17,

3473 (1978).

[36]J. Lindhard and M. Scharff, Phys. Rev. 124, 128 (1961).

[37]O. B. Firsov, Sov. Phys.-JETP 36, 1517 (1959).

[38]P. Sigmund, in *Radiation Damage Processes in Materials*, edited by C. H. S. Dupuy (Noordhoff, Leyden, 1975), p. 3.

[39]K. B. Winterbon, Can. J. Phys. 46, 2429 (1968).

[40]P. Hvelplund and B. Fastrup, Phys. Rev. 165, 408 (1968).

[41]V. B. Ndocko-Ndongue, A. J. Pape, and R. Armbruster, Radiat. Eff. 33, 91 (1977).

[42]L. C. Northcliffe and R. F. Schilling, Nucl. Data 7, 233 (1970).

[43]D. K. Brice, *Ion Implantation Range and Energy Deposition Distributions* (Plenum, New York, 1975), Vol. 1.

[44]R. Weissmann and P. Sigmund, Radiat. Eff. 19, 7 (1973).

[45]J. E. Robinson and S. Agamy, in *Atomic Collisions in Solids*, edited by S. Datz *et al*. (Plenum, New York, 1975), p. 215.

[46]J. Bottiger, J. A. Davies, P. Sigmund, and K. B. Winterbon, Radiat. Eff. 11, 69 (1971).

[47]H. E. Schiott, Radiat. Eff. 6, 107 (1970).

[48]D. K. Brice (unpublished).

[49]H. J. Wollenberger, in *Vacancies and Interstitials in Metals*, edited by A. Seeger *et al*. (North-Holland, Amsterdam, 1970), p. 215.

[50]J. Wurm, F. Dworschak, H. Schuster, and H. Wollenberger, Radiat. Eff. 5, 117 (1970).

[51]J. B. Gibson, A. N. Goland, M. Milgram, and G. H. Vineyard, Phys. Rev. 120, 1229 (1960).

[52]C. Erginsoy, G. H. Vineyard, and A. Englert, Phys. Rev. 133, A595 (1964).

[53]C. Erginsoy, G. H. Vineyard, and A. Shimizu, Phys. Rev. 139, A118 (1965).

[54]C. Erginsoy, in *Interaction of Radiation with Solids*, edited by R. Strumane *et al*. (North-Holland, Amsterdam, 1964), p. 51.

[55]J. O. Schiffgens and R. D. Bourquin, J. Nucl. Mater. 69, 790 (1978).

[56]R. S. Averback, L. J. Thompson, and K. L. Merkle, J. Nucl. Mater. 69, 714 (1978).

[57]R. S. Averback and K. L. Merkle, Phys. Rev. B 16, 3860 (1977).

[58]M. W. Guinan and R. N. Stuart (private communication).

[59]K. L. Merkle, in *Radiation Damage in Metals*, edited by N. L. Peterson and S. D. Harkness, (American Society for Metals, Metals Park, Ohio, 1976), p. 58.

[60]R. C. Birtcher and T. H. Blewitt (private communication).

[61]J. B. Roberto, C. E. Klabunde, J. M. Williams, R. R. Coltman, M. J. Saltmarsh, and C. B. Fulmer, Appl. Phys. Lett. 30, 511 (1977).

[62]M. W. Guinan and C. E. Violet (private communication).